Supporting information for:

Synergistic Control of Multilength-Scale Morphology and Vertical Phase Separation for High-Efficiency Organic Solar Cells

Xiaoli Zhou,[a] Wenting Liang,[a] Ruijie Ma,[b] Cuifen Zhang,[ac] Zhengxing Peng,[d] Top Archie Dela Peña,[e] Jiaying Wu,[e] Zaifei Ma,[c] Yaozu Liao,[a] Gang Li,[b] Huawei Hu*[a]

[a] State Key Laboratory for Modification of Chemical Fibers and Polymer Materials, College of Materials Science and Engineering, Donghua University, Shanghai 201620, China.

E-mail: huaweihu@dhu.edu.cn

[b] Department of Electrical and Electronic Engineering, Research Institute for Smart Energy (RISE), Guangdong-Hong Kong-Macao (GHM) Joint Laboratory for Photonic-Thermal-Electrical Energy Materials and Devices, The Hong Kong Polytechnic University, Hung Hom, Kowloon, Hong Kong, 999077 P. R. China

[c] Center for Advanced Low-Dimension Materials, Donghua University, Shanghai 201620, China

[d] Advanced Light Source, Lawrence Berkeley National Laboratory, Berkeley, CA 94720, USA

[e] Function Hub, Advanced Materials Thrust, The Hong Kong University of Science and Technology, Nansha, 511400 Guangzhou, P. R. China

Molecular properties characterization (UV-vis spectra, TGA, and CV):

The UV-Vis absorption spectra of the solution and film were acquired on a Shimadzu UV-1200 Spectrophotometer. Film samples were spin-cast on ITO substrates. Thermogravimetric analysis (TGA) was carried out on a WCT-2 thermal balance under nitrogen protection at a heating rate of 10 ^{o}C/min. UV-Vis absorption spectra were collected from the solution of the two polymers with a concentration of 0.02 mg/mL in chloroform at different temperatures. Cyclic voltammetry was carried out on a Interface1000E electrochemical workstation with three electrodes configuration, using Ag/AgCl as the reference electrode, a Pt plate as the counter electrode, and a glassy

carbon as the working electrode, in a 0.1 mol/L tetrabutylammonium hexafluorophosphate acetonitrile solution. Potentials were referenced to the ferrocenium/ferrocene couple by using ferrocene as external standards in acetonitrile solutions. The HOMO energy levels were determined by $E_{HOMO} = -[q\,(E_{re} - E_{ferrocene}) + 4.8\ eV]$, while the LUMO energy levels were determined by $E_{LUMO} = -[q\,(E_{ox} - E_{ferrocene}) + 4.8\ eV]$.

Surface Energy: Contact angle measurements were carried out by an Attension Theta Flex meter, using water and ethylene glycol by sessile drop analysis. The surface tension values of films are calculated according to the previous report[1], in which:

$$\gamma_{Water}(\cos\theta_{Water} + 1) = \frac{4\gamma_{water}^{p} \times \gamma^{p}}{\gamma_{water}^{p} + \gamma^{p}} + \frac{4\gamma_{water}^{d} \times \gamma^{d}}{\gamma_{water}^{d} + \gamma^{d}}$$

$$\gamma_{EG}(\cos\theta_{EG} + 1) = \frac{4\gamma_{EG}^{p} \times \gamma^{p}}{\gamma_{EG}^{p} + \gamma^{p}} + \frac{4\gamma_{EG}^{d} \times \gamma^{d}}{\gamma_{EG}^{d} + \gamma^{d}}$$

$$\gamma = \gamma^{d} + \gamma^{p}$$

where θ is the contact angle of each thin film, and γ is the surface tension of samples, which is equal to the sum of the dispersion (γ^{d}) and polarity (γ^{p}) components; γ_{water} and γ_{EG} are the surface tensions of the water and ethylene glycol; and γ_{water}^{d}, γ_{water}^{p}, γ_{EG}^{d} and γ_{EG}^{p} are the dispersion and polarity components of γ_{Water} and γ_{EG}.

Fabrication and testing of Polymer:SMA devices: The best performance for the polymer:SMA devices was achieved after extensive optimization with an inverted structure of ITO/2PACz/polymer:SMA/PNDIT-F_3N/Ag and the details are as follows. Pre-patterned ITO-coated glass with a sheet resistance of ~15 Ω per square was used as the substrate. It was cleaned by sequential sonication in soap DI water, DI water, acetone and isopropanol for 15 min at each step. After ultraviolet/ozone treatment for 60 min, a 2PACz hole transport layer was prepared by spin coating at 4000 r.p.m. Active layers were spin coated from the polymer: NFAs solution to obtain thicknesses of ~100 nm. Polymer: NFAs active layers were cast from chloroform solution (0.7 vol% CN as additive) with 7 mg/mL polymer concentration and 1:1.2 D/A ratio. The thermally annealed polymer: NFAs films were then annealed at 100 °C for 10 min followed by spin coating of a thin layer of PNDIT-F_3N. Then the substrates are transferred to the vacuum chamber of a thermal evaporator inside the glove box and 100 nm of Ag was deposited as the top electrode. All cells were measured inside the glove box. For device characterizations, *J-V* characteristics were measured under AM1.5G light (100 mWcm^{-2}) using a Class AAA Newport solar simulator. The light

intensity was calibrated using a standard Si diode (with KG5 filter, purchased from PV Measurement) to bring spectral mismatch to unity. *J-V* characteristics were recorded using a Keithley 236 source meter unit.

Electron and hole mobility measurements. The electron mobilities were measured using the SCLC method, employing a device architecture of ITO/ZnO/active layer /PNDIT-F3N/Ag The hole-mobilities were measured using a device architecture of ITO/PEDOT:PSS/active layer/MoO_3/Ag. The mobilities were obtained by taking current-voltage curves and fitting the results to a space charge limited form, where the SCLC is described by:

$$J = \frac{9\varepsilon_0\varepsilon_r\mu(V_{appl} - V_{bi} - V_s)^2}{8L^3}$$

Where ε_0 is the permittivity of free space, ε_r is the relative permittivity of the material (assumed to be 3), μ is the hole mobility and L is the thickness of the film. From the plots of $J^{1/2}$ vs $V_{appl} - V_{bi} - V_s$, electron mobilities can be deduced.

Transient absorption spectroscopy.[2] A 50% of the output of a 1 kHz, 1W, 100 fs Ti: sapphire laser system with a 827 nm fundamental (Tsunami oscillator/Spitfire amplifier, Spectra-Physics LLC) was used to pump a commercial collinear optical parametric amplifier (TOPAS-Prime, Light-Conversion LLC) tuned to 800. The pump was depolarized to suppress effects due to polarization-dependent dynamics and attenuated to the specific energy density. The pump was focused to a 1 mm diameter spot at the sample position. The probe was generated using 10% of the remaining output to drive continuum generation in a proprietary crystal and detected on a commercial spectrometer (customized Helios, Ultrafast Systems LLC).

AFM characterization: AFM measurements were performed by using a Scanning Probe Microscope Dimension 3100 in tapping mode. All film samples were spin-cast on ITO substrates.

GIWAXS characterization: GIWAXS measurements were performed at beamline BL16B1 at the Shanghai Synchrotron Radiation Facility. Samples were prepared on Si substrates using identical blend solutions as those used in devices. The 10 KeV X-ray beam was incident at a grazing angle of 0.13°, which maximized the scattering intensity from the samples. The scattered X-rays were detected using a Dectris Pilatus 1-M

photon counting detector. Samples were prepared on Si substrates. In-plane and out-of-plane sector averages were calculated using the Nika software package. The uncertainty for the peak fitting of the GIWAXS data is 0.3 Å. The coherence length was calculated using the Scherrer equation: CL=2π*K*/Δ*q*, where Δq is the full-width at half-maximum of the peak and K is a shape factor (0.9 was used here).[3]

Trap density of states: Trap density of states (tDOS) were performed on Keysight 4980A and analyzed by using the thermal admittance spectroscopy (TAS) method under angular frequency-dependent capacitance measurement (0.02 kHz to 2000 kHz). The energetic profile of tDOS of solar cells can be derived according to the following equation:

$$N_T(E_\omega) = -\frac{V_{\mathrm{bi}}}{qW}\frac{dC}{d\omega}\frac{\omega}{k_{\mathrm{B}}T}$$

where k_{B} is the Boltzmann's constant, ω is the angular frequency, C is the capacitance, T is the absolute temperature, W is the depletion width, and V_{bi} is the built-in potential. The applied angular frequency ω is defined by the following formula:

$$E_\omega = k_{\mathcal{B}}T\ln(\frac{\omega_0}{\omega})$$

where ω_0 is the attempt-to-escape frequency. The trap states below the energy demarcation can capture or emit charges with the given ω and contribute to the capacitance.

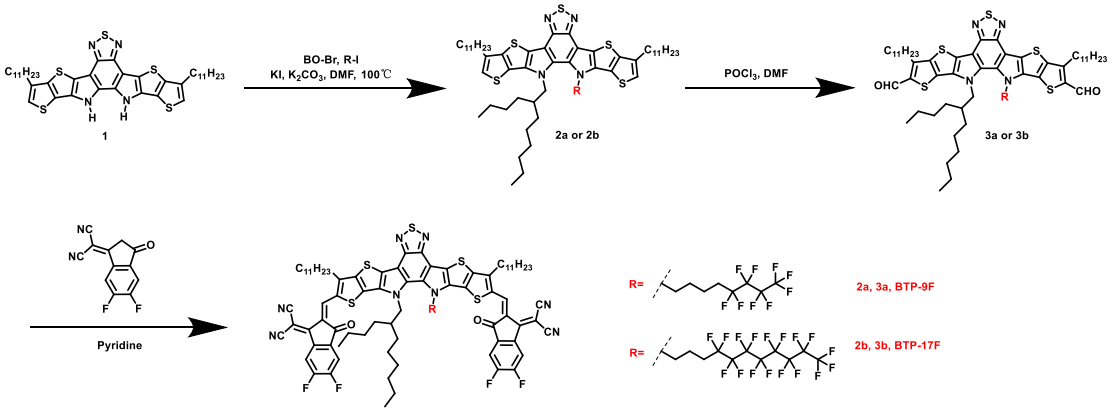

Scheme S1. Synthetic route for BTP-9F and BTP-17F.

Table S1. Basic parameters for BTP-9F and BTP-17F.

Materials	λ_{max} [a] [nm]	λ_{max} [b] [nm]	λ_{onset} [b] [nm]	E_g^{opt} [c] [eV]	LUMO/HOMO [d] [eV]	E_g^{ele} [e] [eV]	T_d [℃]
BTP-9F	725	806	850	1.46	-3.93/-5.68	1.75	340.3
BTP-17F	721	801	844	1.47	-3.94/-5.71	1.77	347.4

[a] In solution state (Chloroform). [b] In pure films. [c] Obtained with $E_g^{opt} = 1240/\lambda_{onset}$ [b]. [d] Measured by cyclic voltammetry (CV) method. [e] Obtained with equation: E_g^{ele} = LUMO-HOMO.

Table S2. The CCL and d-spacing values of BTP-9F, BTP-17F films.

Film	q_0 (Å^{-1})	d (Å)	CCL (Å)
BTP-9F	1.74	3.59	36.3
BTP-17F	1.73	3.61	33.9
BTP-eC9	1.74	3.59	29.6
BTP-eC9: BTP-9F (1:0.2)	1.74	3.59	35.0

Table S3. The optimal photovoltaic parameters of eC9-based binary and ternary OSCs.

Active layer	V_{OC} (V)	J_{SC} (mA cm^{-2})	FF (%)	PCE (%)
PM6:BTP-eC9 (1:1.2)	0.846	27.6	77.2	18.0
PM6:BTP-eC9: BTP-9F (1:1.1:0.1)	0.848	27.8	78.1	18.4
PM6:BTP-eC9: BTP-9F (1:1:0.2)	0.850	28.0	79.9	19.1
PM6: BTP-eC9: BTP-9F (1:0.8:0.4)	0.849	27.8	75.3	17.8

Table S4. The electrical parameters for corresponding devices.

	P_{diss}	P_{coll}	α	n
PM6: BTP-9F	98.7%	88.3%	0.99	1.09
PM6: BTP-17F	97.9%	81.3%	0.99	1.40
PM6: BTP-eC9	98.8%	90.3%	0.98	1.04
PM6: BTP-eC9:BTP-9F	99.4%	91.2%	0.97	1.01

Table S5. The charge mobility of hole or electron-only devices for corresponding blend films.

	μ_h (10^{-4} cm^2 V^{-1} s^{-1})	μ_e (10^{-4} cm^2 V^{-1} s^{-1})	μ_h/μ_e
PM6: BTP-9F	4.0	3.5	1.14
PM6: BTP-17F	2.9	2.2	1.32
PM6: BTP-eC9	4.9	4.4	1.11
PM6: BTP-eC9: BTP-9F	7.0	6.6	1.06

Table S6. Parameters of out-of-plane π-π stacking for donor and acceptor in the corresponding films.

Materials	Donor (010) stacking		Acceptor (010) stacking	
	d (Å)	CCL (Å)	d (Å)	CCL (Å)
PM6: BTP-9F	3.72	31.3	3.61	35.2
PM6: BTP-17F	3.72	28.1	3.64	33.1
PM6: BTP-eC9	3.72	18.8	3.59	31.3
PM6: BTP-eC9: BTP-9F	3.72	28.6	3.59	37.5

Table S7. Parameters of domain purity and domain size in the corresponding films.

Active layer	Relative overall purity	Relative high-q purity	Domain size (nm)	
			low-q	high-q
PM6:BTP-9F	0.98	0.80	95.1	17.8
PM6:BTP-17F	0.85	0.75	125.6	20.9
PM6:BTP-eC9	0.68	0.47	104.6	23.3
Ternary	1	0.69	98.1	18.9

Table S8. Surface energy for pure and blend films calculated from water and ethylene glycol contact angle.

Films	Contact angle (°)		γ_s^d (mJ m^{-2})	γ_s^p (mJ m^{-2})	γ_s (mJ m^{-2})
	H_2O (average)	EG (average)			
PM6	102.5	75.0	25.50	0.48	25.98
BTP-9F	106.6	84.9	17.59	0.66	18.25
BTP-17F	115.4	93.2	15.47	0.11	15.58
BTP-eC9	95.5	64.5	31.57	0.87	32.44
PM6: BTP-9F	104.2	77.8	23.56	0.45	24.01
PM6: BTP-17F	108.1	86.2	16.43	0.75	17.18
PM6: BTP-eC9	100.6	72.1	27.30	0.55	27.85
Ternary	103.6	76.2	25.22	0.38	25.60

Table S9. Detailed energy loss analysis of OSCs devices.

Active layer	E_g (eV)	$V_{oc,sq}$ (V)	ΔE_1 (eV)	$V_{oc,rad}$ (V)	ΔE_2 (eV)	ΔE_3 (eV)	E_{loss} (eV)
PM6: BTP-9F	1.457	1.191	0.266	1.112	0.079	0.264	0.609
PM6: BTP-17F	1.466	1.200	0.266	1.117	0.083	0.285	0.634
PM6: BTP-eC9	1.428	1.161	0.267	1.092	0.069	0.246	0.582
Ternary	1.428	1.166	0.262	1.095	0.071	0.245	0.578

[a] $V_{oc,sq}$: Schokley−Queisser limit to V_{OC}. [b] $V_{oc,rad}$: V_{OC} when there is only radiative recombination.

Table S10. Photovoltaic parameters of the optimized OSCs based on PM6:Y6 and PM6:L8-BO and corresponding ternary OSCs with the addition of 10 wt% BTP-9F.

Active layer	V_{OC} (V)	J_{SC} (mA cm^{-2})	J_{sat} (mA cm^{-2})	FF (%)	PCE (%)
PM6:Y6	0.831 [0.831±0.003]	27.4 [26.9±0.3]	27.1	74.1 [74.7±0.4]	16.9 [16.6±0.3]
PM6:Y6:BTP-9F	0.836 [0.836±0.002]	27.9 [27.5±0.4]	27.4	77.5 [77.0±0.5]	18.1 [17.8±0.3]
PM6:L8-BO	0.888 [0.888±0.002]	26.6 [26.4±0.3]	25.7	75.4 [75.2±0.4]	17.8 [17.5±0.3]
PM6:L8-BO:BTP-9F	0.886 [0.886±0.002]	26.9 [26.5±0.4]	25.9	78.8 [78.3±0.5]	18.8 [18.4±0.4]

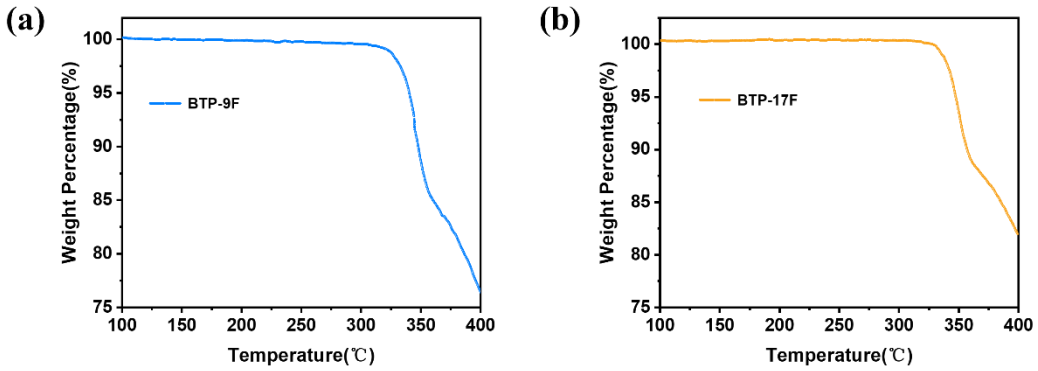

Figure S1. Thermogravimetric analysis (TGA) curve of (a) BTP-9F and (b) BTP-17F measured with a heating rate of 10 °C/ min under N_2 atmosphere.

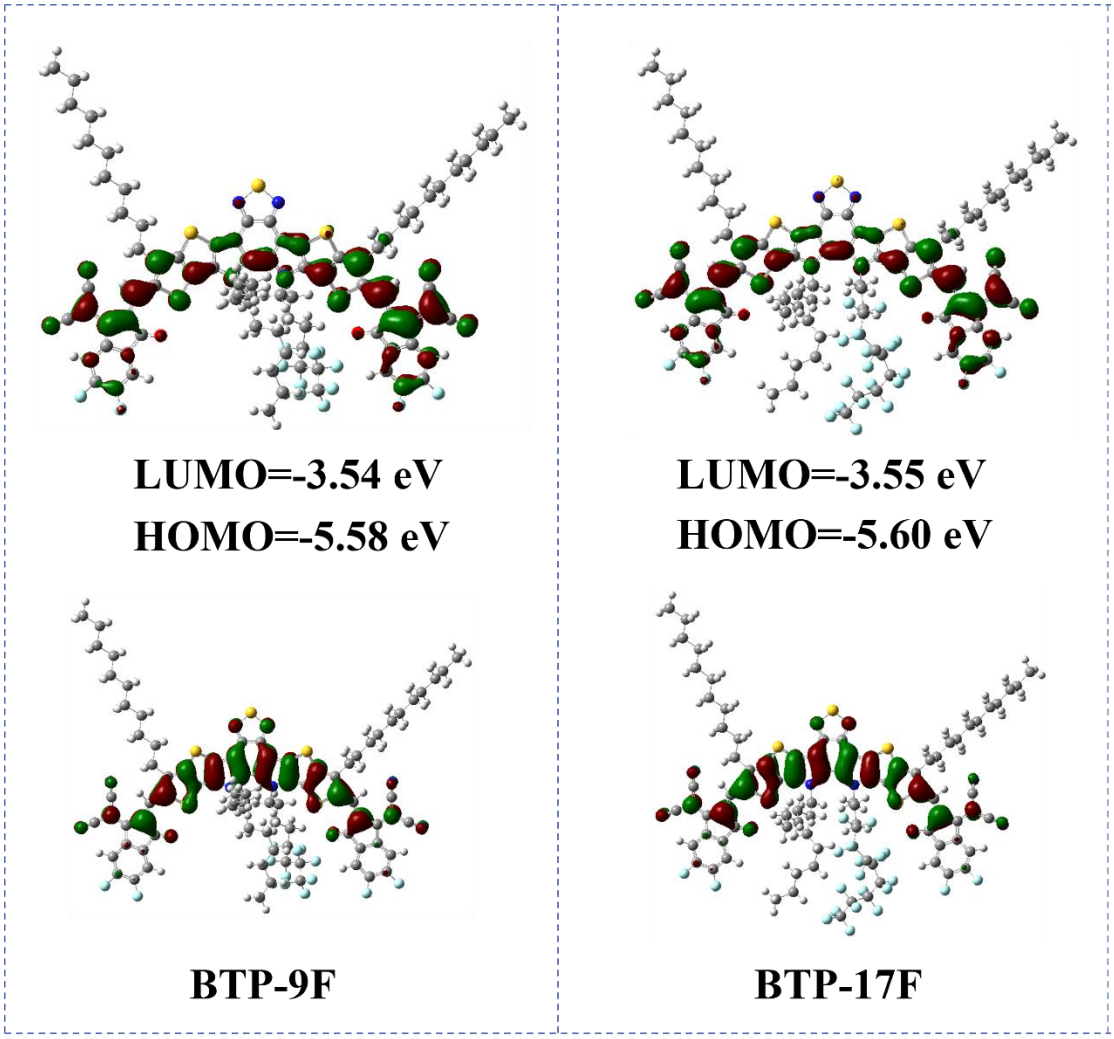

Figure S2. the HOMO and LUMO energy levels of BTP-9F and BTP-17F.

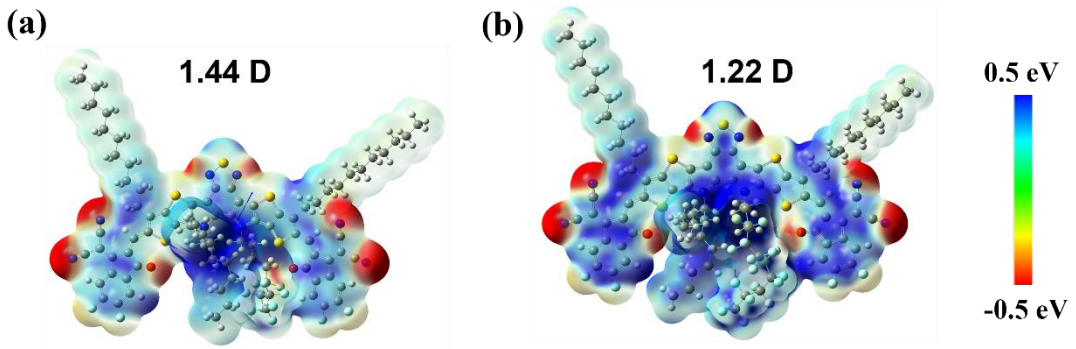

Figure S3. The ESP plots of (a) BTP-9F and (b) BTP-17F.

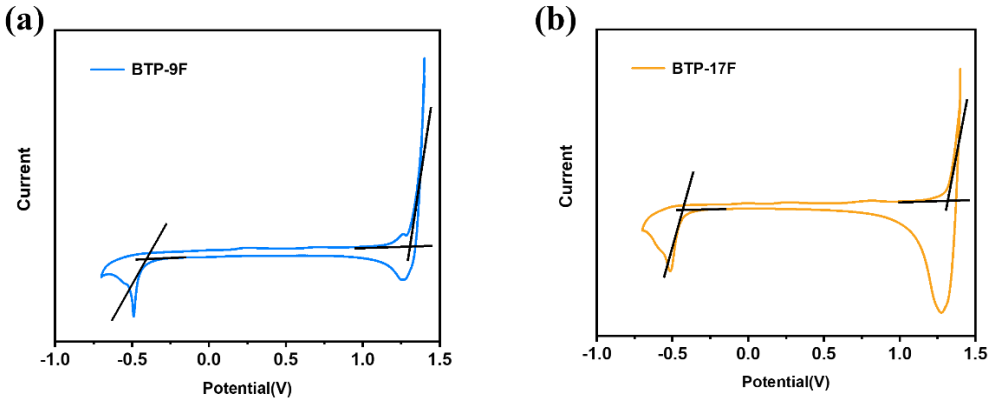

Figure S4. The CV plots of (a) BTP-9F and (b) BTP-17F.

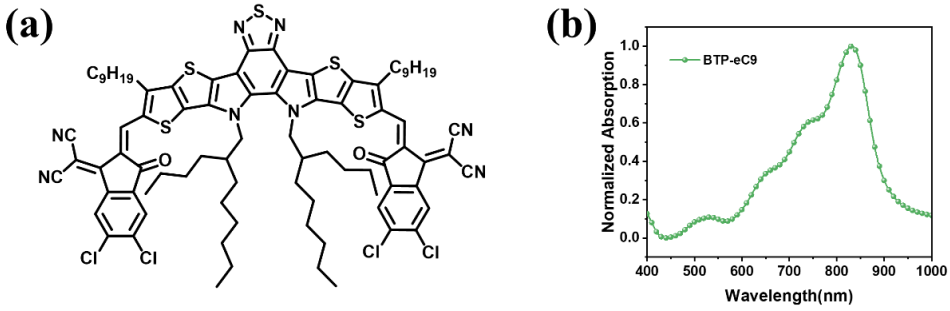

Figure S5. (a) Chemical structures and (b) normalized absorption of BTP-eC9.

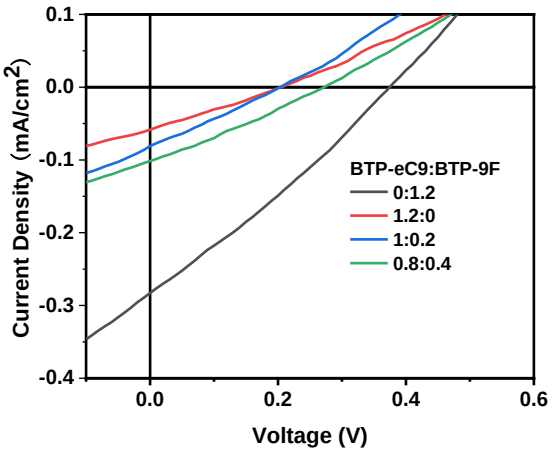

Figure S6. *J–V* curves of acceptor-only devices.

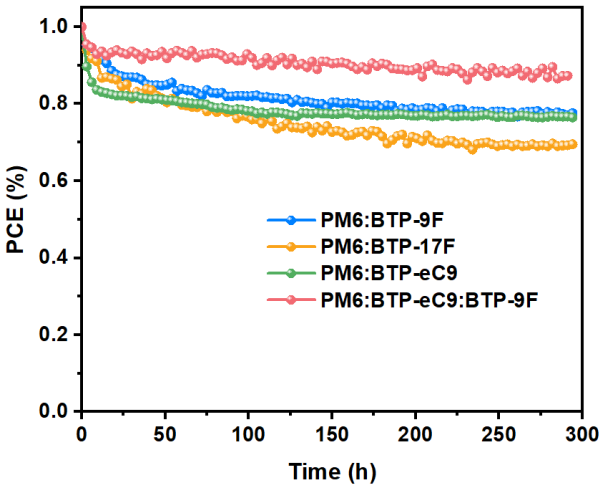

Figure S7. Photostability of the encapsulated devices with MPP tracking under 1-sun illumination.

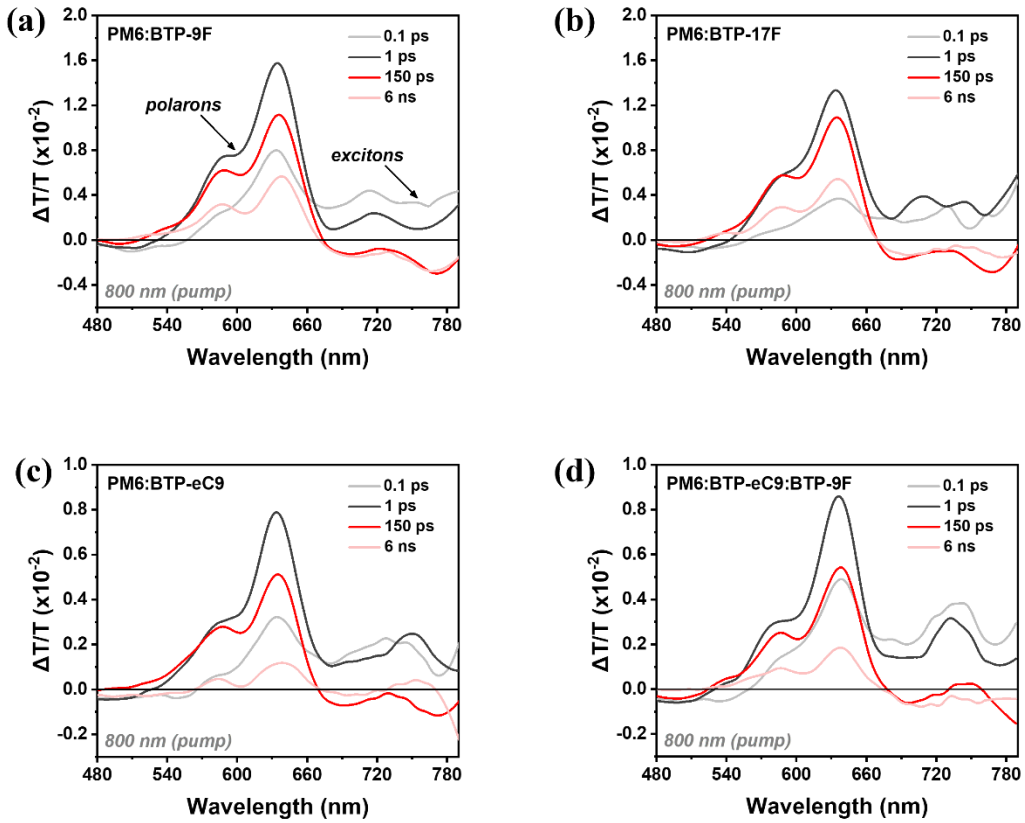

Figure S8. The representative spectrum at the specified delay time and decay dynamics monitored at the 800nm of blend films.

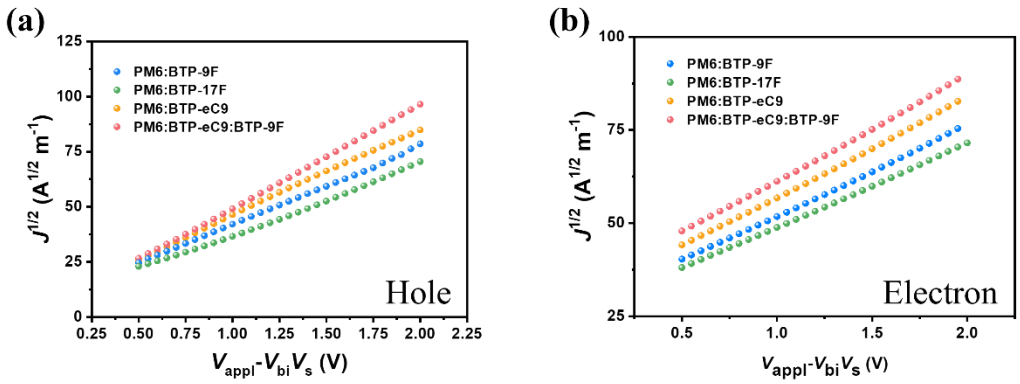

Figure S9. (a) Hole and (b) Electron current densities with applied voltage in selective carrier injected diodes.

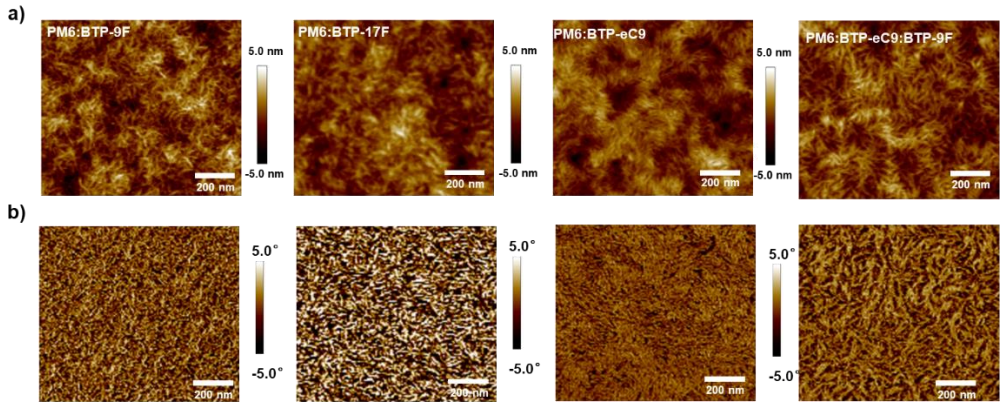

Figure S10. The AFM height images (a, top) and phase (b, Bottom) images for the corresponding blend films.

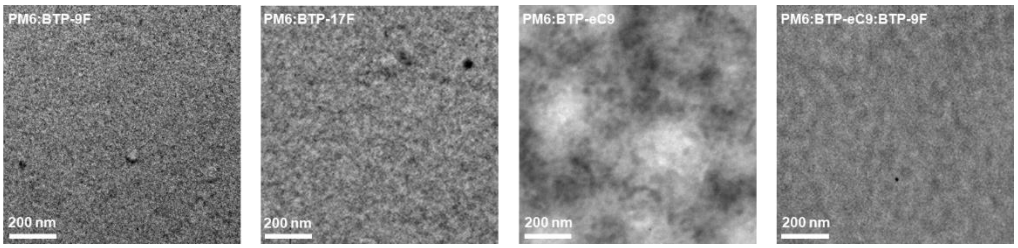

Figure S11 TEM images for PM6:BTP-9F, PM6:BTP-17F, PM6:BTP-eC9, and PM6:BTP-eC9:BTP-9F-based blend films.

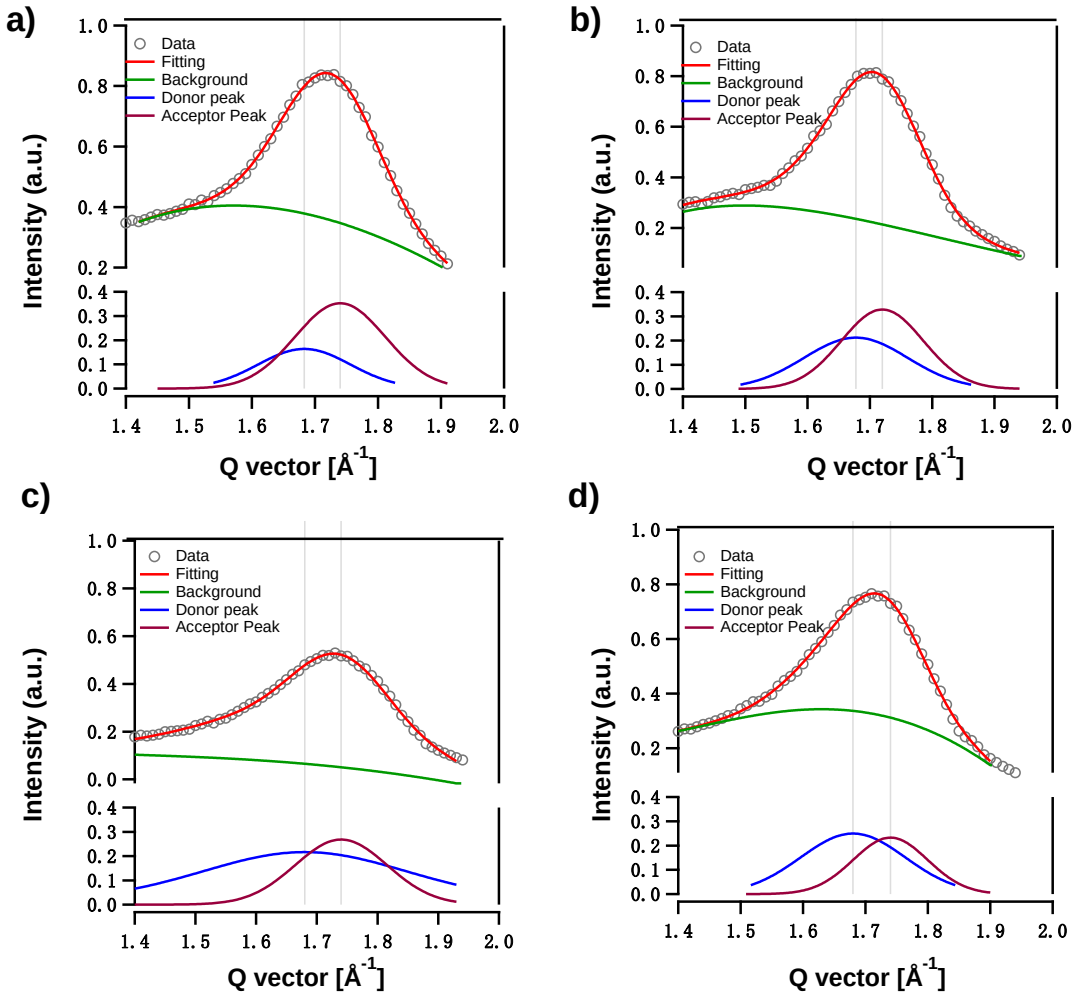

Figure S12. Multi-peak fitting of the GIWAXS profiles of (a) PM6:BTP-9F; (b) PM6:BTP-17F; (c) PM6:BTP-eC9; (d) PM6:BTP-eC9:BTP-9F-based blend films.

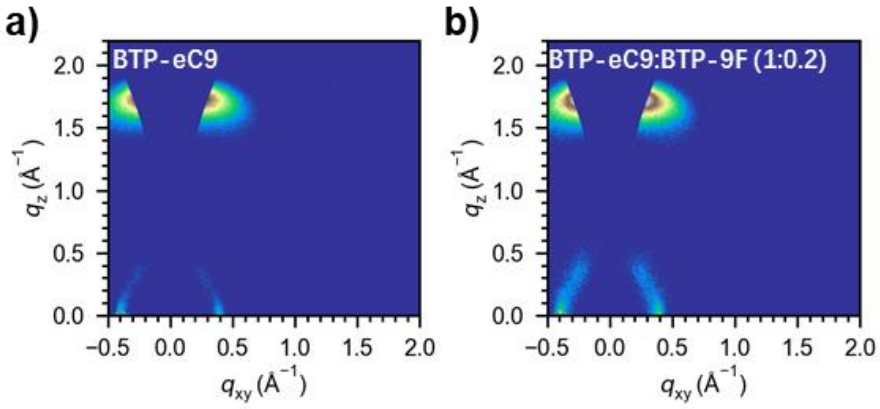

Figure S13. 2D GIWAXS patterns for (a) BTP-eC9 and (b) BTP-eC9:BTP-9F-based films.

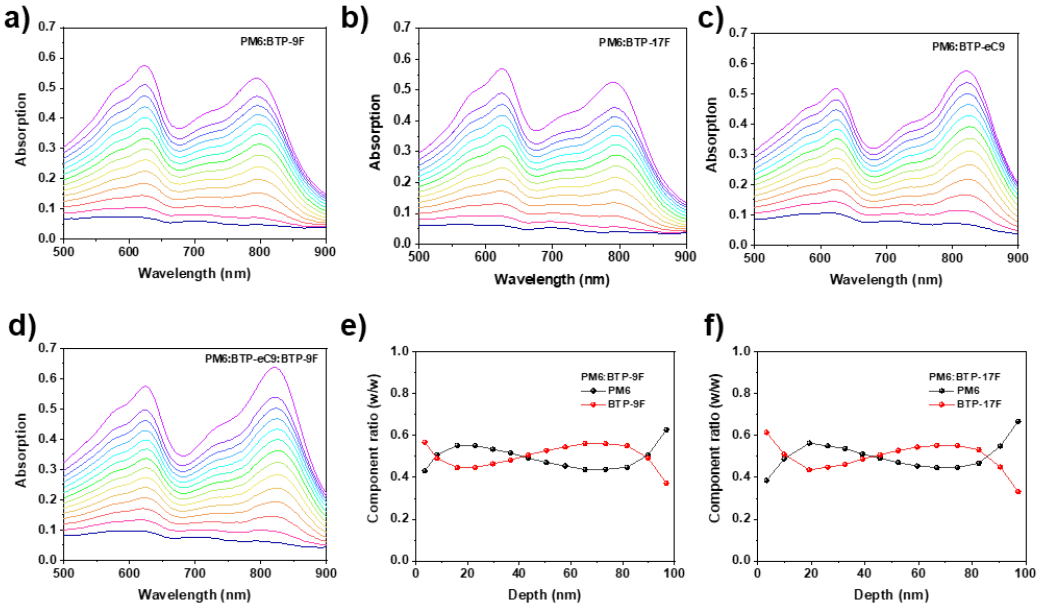

Figure S14. (a-d) The film-depth-dependent profiling light absorption spectra. (e,f) Derived weight-ratio vertical distribution within the blend films.

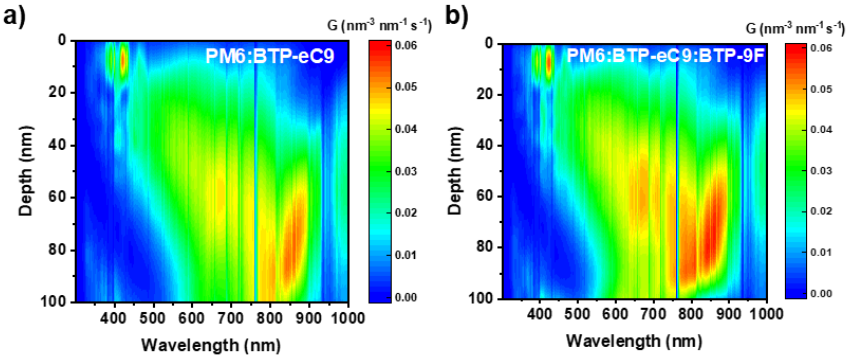

Figure S15. Exciton generation contours as numerically for (a) PM6:BTP-eC9 and (b) PM6:BTP-eC9:BTP-9F-based blend films.

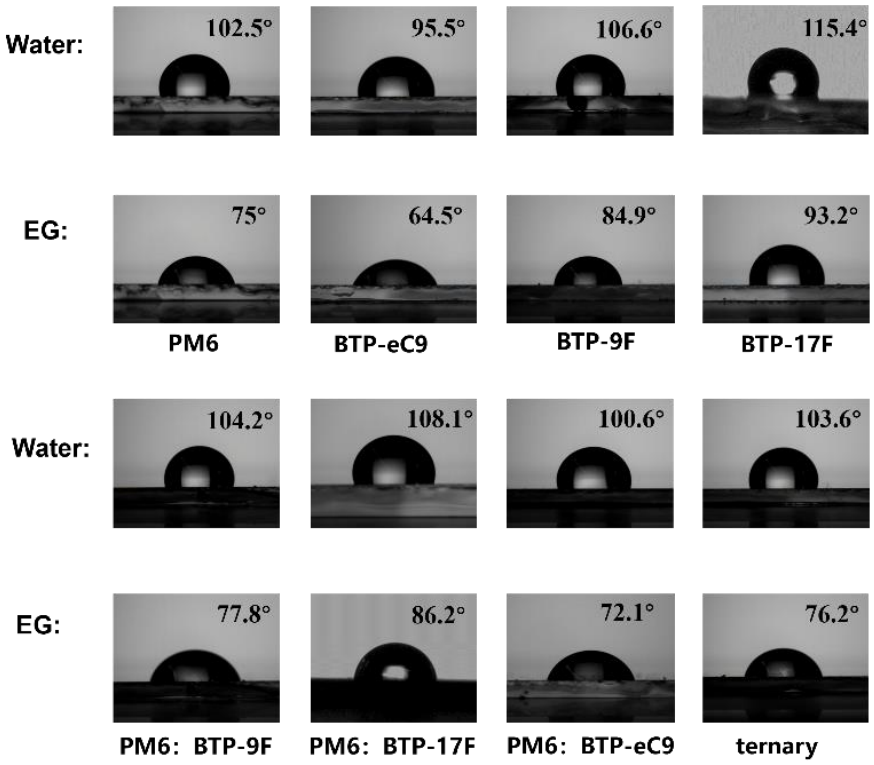

Figure S16. Photographs of water and ethylene glycol droplets on the top surface of corresponding films.

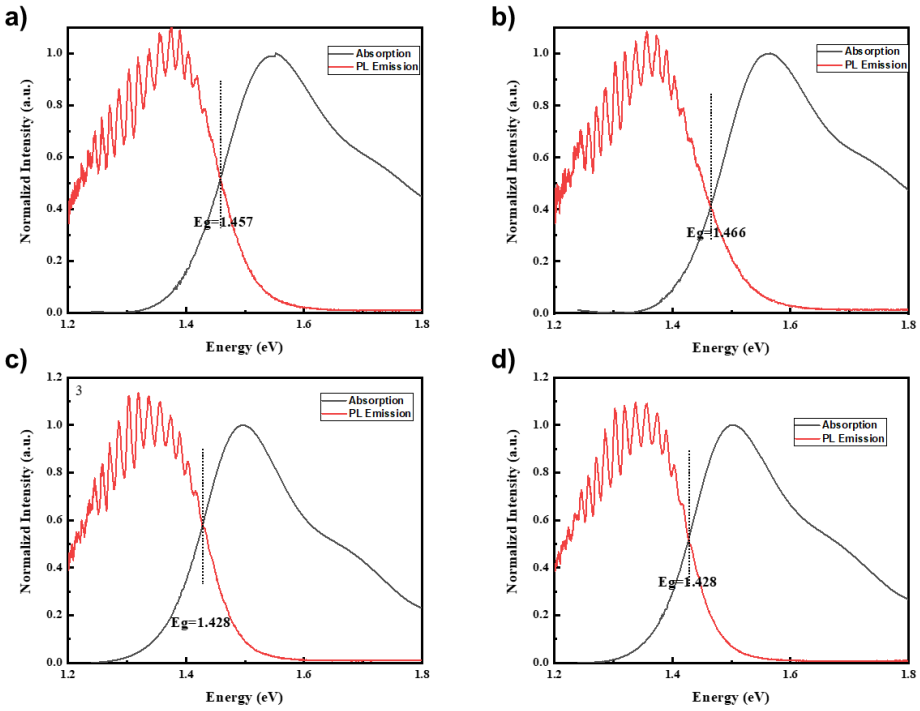

Figure S17. Details of optical Eg determination. Eg is estimated by the cross-point of normalized absorption (black lines) and photoluminescence (PL) spectra (red lines) of the corresponding films.

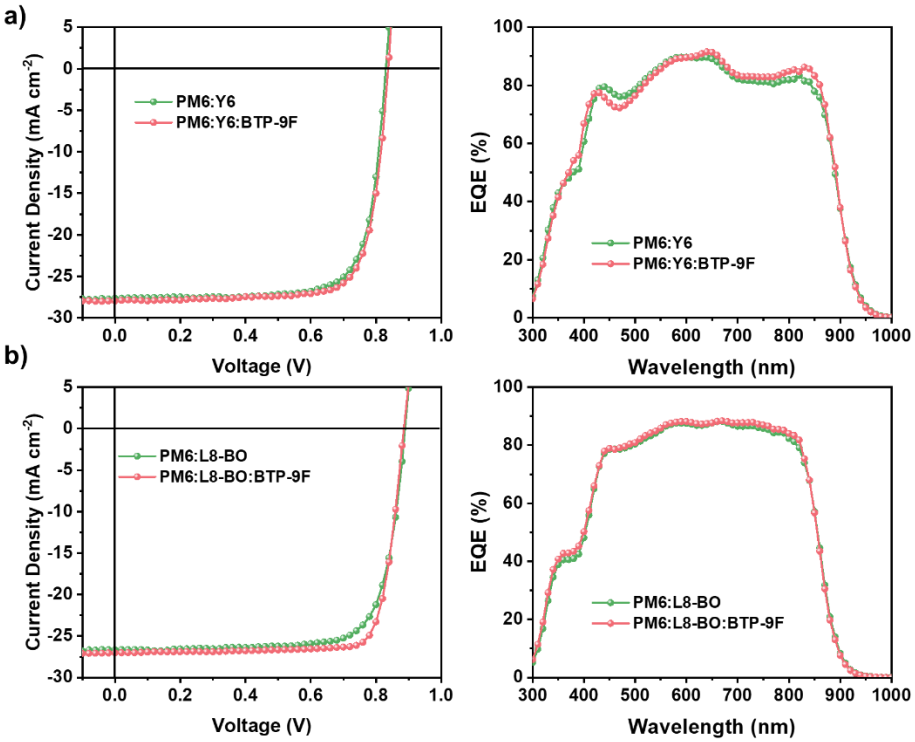

Figure S18. *J-V* and EQE for (a) PM6:Y6 and PM6:Y6:BTP-9F, and (b) PM6:L8-BO and PM6:L8-BO:BTP-9F.

Materials and synthesis

All chemicals, unless otherwise specified, were purchased from Aldrich or other commercial resources and used as received. Toluene was distilled from sodium benzophenone under nitrogen before using.

^{1}H and ^{13}C NMR spectra were recorded on Bruker AV-400 MHz NMR spectrometer or Bruker AV-600 MHz NMR spectrometer. Chemical shifts are reported in parts per million (ppm, δ). ^{1}H NMR and ^{13}C NMR spectra were referenced to tetramethylsilane (0 ppm) for $CDCl_3$. Mass spectra were collected on a MALDI Micro MX mass spectrometer, or an API QSTAR XL System.

Synthesis of compound 2a: To a two-neck flask containing compound 1 (558 mg, 0.7 mmol), 5-(Bromomethyl)undecane (279 mg, 1.1 mmol), 4-(perfluorobutyl)butyliodide (286 mg, 0.7 mmol), KI (124 mg, 0.75 mmol), K_2CO_3 (491 mg, 3.6 mmol), and dried DMF (15 ml) were added under N_2 atmosphere. The reaction was stirred at 100 ℃ for 12 h. After cooling to room temperature, the reaction was extracted with ethyl acetate three times. The organic layers were combined and washed with saturated brine, and dried over Na_2SO_4. After evaporation of the solvent, the residue was purified by column

chromatography (PE/DCM = 10/1) to give the corresponding product 2 as an orange oil in 30% yield (423 mg).

^{1}H NMR (400 MHz, $CDCl_3$) δ7.02 (s, 2H), 4.69-4.63 (m, 2H), 4.60-4.57 (m, 2H), 2.81 (t, J = 7.6 Hz, 4H), 2.09 (d, J = 5.5 Hz, 2H), 1.89-1.85 (m, 4H), 1.86-1.81 (m, 4H), 1.44 -1.28 (m, 31H), 1.09-1.05 (m, 3H), 1.01-0.95 (m, 7H), 0.90-0.84 (m, 14H), 0.67 (m, 6H).

^{13}C NMR (151 MHz, $CDCl_3$) δ 147.61, 147.43, 142.47, 142.25, 137.18, 137.12, 137.06, 136.78, 131.38, 131.10, 123.62, 123.32,123.07, 122.91, 119.51, 119.30, 117.81, 116.36, 112.20, 112.19, 111.58, 110.29, 108.06, 106.99, 54.80, 50.58, 38.74, 31.94, 29.70, 29.66, 29.63, 29.51, 29.49, 29.47, 29.38, 25.20, 22.73, 22.71, 22.44, 17.48, 14.13, 13.92, 13.69.

MS (MALDI-TOF) m/z calcd. for ($C_{60}H_{81}F_9N_4S_5$): 1188.4921. Found:1188.4927

Synthesis of Compound 2b: The detailed synthetic procedure of compound 2b was similar to that of compound 2a. The little difference is that the 4-(perfluorobutyl)butyliodide used in the synthetic procedure of compound 2a was replaced with 3-(perfluorooctyl)propyliodide (434 mg, 0.74 mmol). The final product compound 2b was obtained as an orange solid (273 mg, 40%).

^{1}H NMR (600 MHz, $CDCl_3$) δ7.03 (s, 2H), 4.72-4.69 (m, 2H), 4.60-4.55 (m, 2H), 2.85 (t, J = 7.6 Hz, 4H), 2.81 (d, J = 5.5 Hz, 2H), 2.15-1.87 (m, 2H), 1.86-1.84 (m, 4H), 1.43 -1.27 (m, 36H), 1.07-0.97 (m, 3H), 1.01-0.94 (m, 6H), 0.89-0.86 (m, 9H), 0.67 (m, 7H).

^{13}C NMR (151 MHz, $CDCl_3$) δ 147.55, 147.29, 142.54, 142.28, 137.07, 136.99, 136.95, 136.74, 131.25, 131.03, 123.60, 123.57,122.99, 122.94, 119.55, 119.39, 118.19, 118.08, 117.98, 116.31, 116.16, 112.47, 112.09, 111.62, 110.82, 110.66, 110.45, 108.01, 106.67, 54.66, 50.04, 38.77, 31.95, 31.51, 29.71, 29.70, 29.66, 29.64, 29.62, 29.59, 29.54, 29.50, 29.47, 29.38, 29.30, 28.81, 28.77, 25.23, 22.71, 22.59, 22.43, 21.92, 14.11, 13.88, 13.84, 13.64.

MS (MALDI-TOF) m/z calcd. for ($C_{63}H_{79}F_{17}N_4S_5$): 1374.4637. Found:1374.4636.

Synthesis of compound 3a: Under N_2 atmosphere, $POCl_3$ (1 mL) was slowly added to dried DMF (2 mL) in a two-neck flask. After stirring at 0 ℃ for 0.5 h, a solution of compound 2 (77 mg, 0.06 mmol) in dried DCM (3 mL) was added to the reaction mixture and stirred for 12 h at 80 ℃. The reaction mixture was poured into K_2CO_3 aqueous solution (10 mL) slowly and then extracted with ethyl acetate three times. The organic layers were combined and washed with saturated brine, and dried over Na_2SO_4.

After evaporation of the solvent, the residue was purified by column chromatography (PE/DCM = 2/1) to give the corresponding product 3 as an orange solid in 85% yield (70 mg).

^{1}H NMR (400 MHz, $CDCl_3$) δ 10.15 (s, 2H), 4.75-4.71 (m, 2H), 4.62 (d, J = 7.5 Hz, 2H), 3.22 -3.19 (m, 4H), 2.06 (d, J = 7.8 Hz, 2H), 1.94-1.87 (m, 7H), 1.43-1.26 (m, 34H), 1.08-0.94 (m, 13H), 0.79 (t, J = 7.4 Hz, 6H), 0.66 (m, J = 7.2 Hz, 9H).

^{13}C NMR (151 MHz, $CDCl_3$) 181.77, 181.74, 147.44, 147.26, 147.07,146.96, 146.75, 143.47, 143.27, 143.20, 137.20, 137.10, 136.84, 136.74 , 132.64, 132.44, 129.59, 128.96, 128.03, 127.54,124.38, 123.90, 123.39, 120.33, 117.67, 116.70, 115.72, 113.93, 113.62, 112.94, 112.48, 55.11, 53.49, 50.77, 39.00, 34.91, 34.59, 31.90, 31.47, 30.32, 29.64, 29.60, 29.52, 29.38, 29.37, 29.33, 29.29, 28.16, 25.10, 22.69, 22.46, 17.45, 14.11, 13.82, 13.65.

MS (MALDI-TOF) m/z calcd. for ($C_{62}H_{81}F_9N_4O_2S_5$): 1244.4819. Found:1244.4811

Synthesis of compound 3b:

^{1}H NMR (400 MHz, $CDCl_3$) δ 10.15 (d, 2H), 4.79-4.76 (m, 2H), 4.61-4.59 (d, J = 7.5 Hz, 2H), 3.21-3.18 (m, 4H), 2.13 (d, J = 7.8 Hz, 2H), 1.93-1.91 (m, 7H), 1.37-1.33 (m, 36H), 1.29-1.08 (m, 16H), 0.96-0.85 (t, J = 7.4 Hz, 5H), 0.60 (t, J = 7.2 Hz, 3H).

^{13}C NMR (151 MHz, $CDCl_3$) 181.70, 147.39, 147.35, 147.11, 147.08, 146.92, 146.90, 146.82, 146.67, 146.64, 143.56, 143.28, 143.25, 137.27, 137.16, 136.59, 136.58, 132.53, 132.51, 129.53, 129.51, 128.78, 128.70, 128.32, 128.28, 127.52, 127.48, 127.34, 113.00, 112.98, 112.96, 112.95, 112.75, 112.45, 112.42, 112.16, 54.99, 54.76, 50.29, 39.03, 31.90, 31.45, 29.65, 29.63, 29.60, 29.52, 29.37, 29.36, 29.33, 29.27, 25.13, 25.06, 22.41, 22.35, 22.05, 14.08, 13.87, 13.60.

HR-MS (MALDI-TOF) m/z calcd. for ($C_{65}H_{79}F_{17}N_4O_2S_5$): 1430.4535. Found: 1430.4536

Synthesis of BTP-9F: To a two-neck flask containing compound 3 (42.5 mg, 0.034 mmol), 2-(5,6-difluoro-3-oxo2,3-dihydro-1H-inden-1-ylidene) malononitrile (32 mg, 0.14 mmol), $CHCl_3$ (5 mL) and pyridine (0.5 mL) were added under nitrogen atmosphere. The mixture was stirred at 30 ℃ for 2 h. After evaporation of the solvent, the residue was purified by column chromatography (PE/DCM = 1/1) to give the corresponding product BTP-9F as a dark solid in 65% yield (38 mg).

^{1}H NMR (600 MHz, $CDCl_3$) δ 8.77 (s, 1H), 8.67 (s, 1H), 8.37-8.35 (t, 2H), 7.63-7.60 (t, 1H), 7.54-7.52 (t, 1H), 4.78-4.61 (m, 4H), 3.00-2.93 (m, 5H), 2.48 (s, 5H), 2.11-2.04

(m, 4H), 1.74-1.71 (m, 5H), 1.46 -1.45 (d, 5H), 1.34-1.26 (m, 32H), 0.94-0.85(m,13H), 0.63-0.61 (m, 6H).

^{13}C NMR (151 MHz, $CDCl_3$) δ 185.95, 157.92, 157.57, 155.15, 155.06, 153.71, 153.47, 153.44, 153.41, 153.32, 147.12, 146.89, 145.20, 145.05, 137.02, 136.43, 136.26, 134.94, 134.23, 133.98, 133.93, 133.51, 132.93, 132.46, 132.43, 130.76, 130.55, 119.82, 119.77, 116.48, 114.84. 114.80, 114.71, 114.57, 114.33, 114.31, 113.48, 113.29, 112.33, 112.19, 112.00, 111.79, 109.27, 108.52, 99.99, 69.08, 68.73, 68.71, 55.34, 51.20, 39.34, 39.31, 39.26, 31.93, 31.47, 29.85, 29.79, 29.66, 29.63, 29.51, 29.43, 29.36, 29.28, 25.51, 22.70, 22.38, 21.97, 18.01, 17.99, 14.13, 13,90, 13.65.

HR-MS (MALDI-TOF) m/z calcd. for ($C_{86}H_{85}F_{13}N_8O_2S_5$): 1668.5191. Found:1668.5259.

Synthesis of BTP-17F:

^{1}H NMR (400 MHz, $CDCl_3$) δ 8.83 (s, 1H), 8.66 (s, 1H), 8.40-8.35 (t, 2H), 7.63-7.59 (t, 1H), 7.54-7.45 (t, 1H), 4.82-4.54 (m, 4H), 3.01-2.94 (m, 4H), 2.70 (s, 4H), 2.11-2.03 (m, 1H), 1.95-1.71 (m, 4H), 1.46 -1.45 (d, 4H), 1.34-1.27 (m, 34H), 0.87-0.85(m,15H), 0.63-0.58 (m, 7H).

^{13}C NMR (151 MHz, $CDCl_3$) δ 185.80, 157.74, 157.24, 155.19, 155.16, 153.62, 153.43, 153.41, 153.38, 153.32, 146.97, 146.91, 145.20, 145.01, 136.69, 136.66, 136.35, 136.66, 134.66, 134.35, 134.30, 134.23, 133.69, 133.65, 133.36, 132.88, 132.39, 132.00, 130.86, 130.57, 119.81, 119.77, 114.91, 114.76. 114.72, 114.71, 114.59, 114.57, 114.44, 114.34, 114.25, 113.31, 113.18, 112.22, 112.10, 111.67, 111.65, 111.54, 69.46, 69.45, 68.85, 55.13, 55.09, 50.56, 39.37, 31.94, 31.42, 31.00, 30.77, 30.55, 29.86, 29.78, 29.66, 29.64, 29.51, 29.42, 29.37, 29.22, 23.08, 22.71, 22.62, 22.35, 14.13, 13,84, 13.54.

HR-MS (MALDI-TOF) m/z calcd. for ($C_{89}H_{83}F_{21}N_8O_2S_5$): 1854.4907. Found:1854.4415.

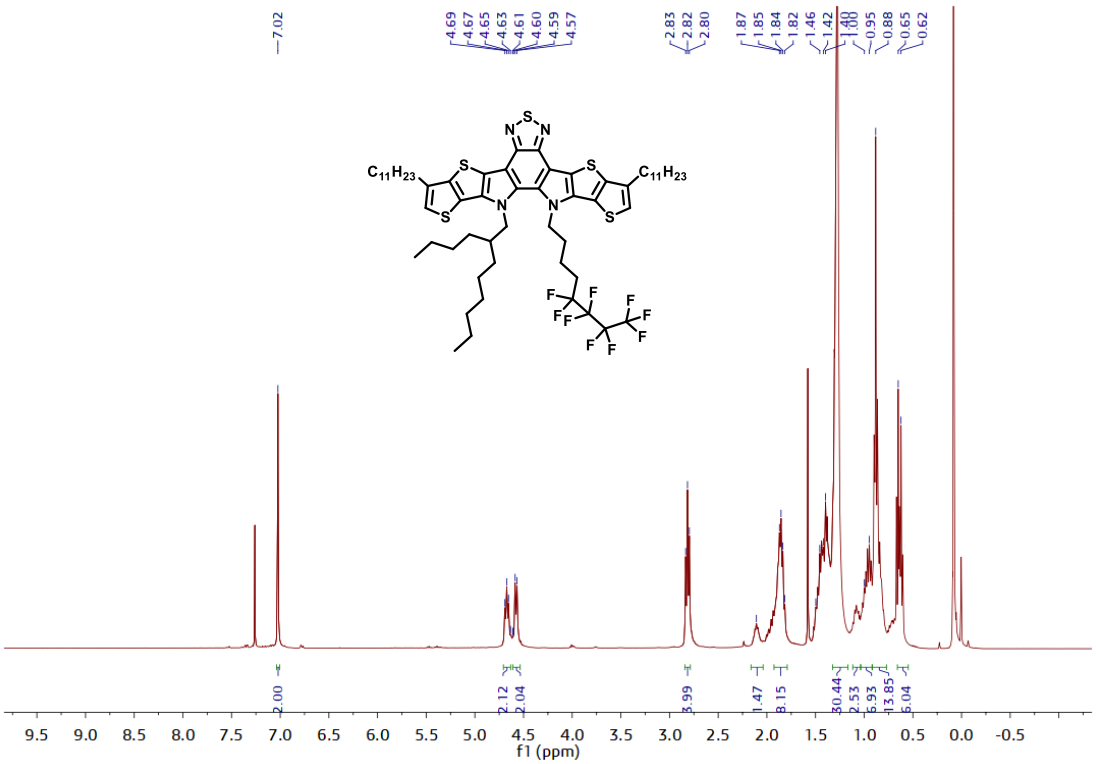

Figure S19. ^{1}H NMR spectrum of Compound 2a

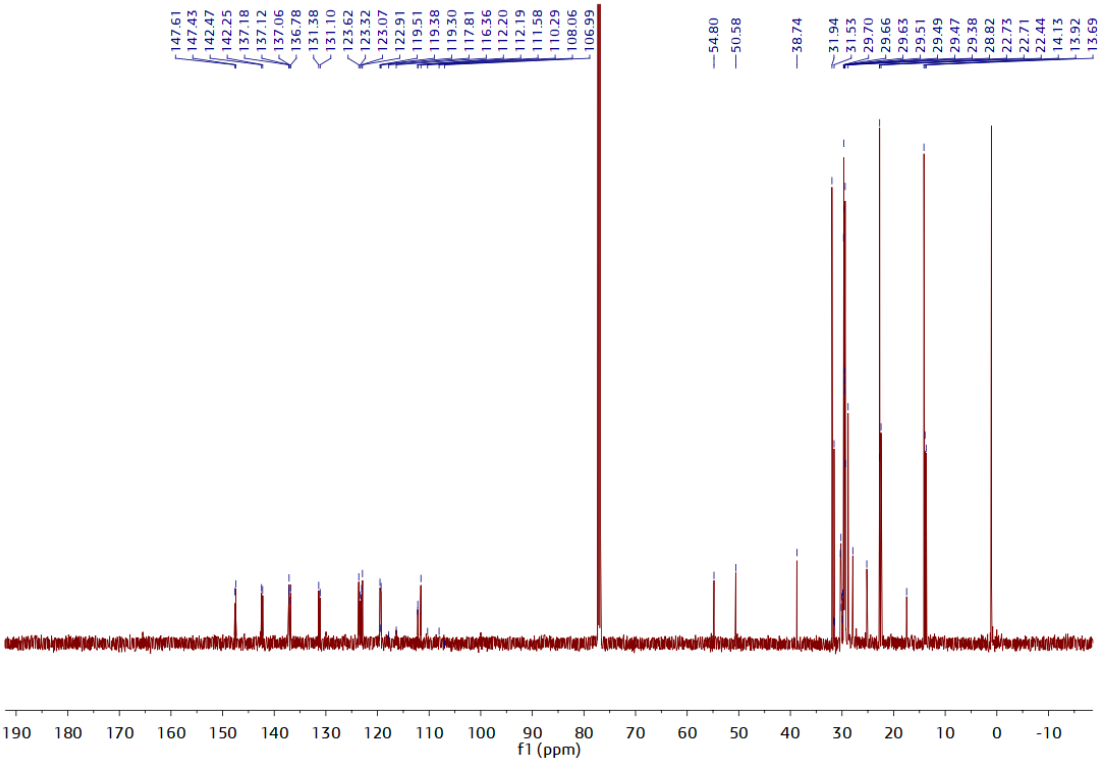

Figure S20. ^{13}C NMR spectrum of Compound 2a

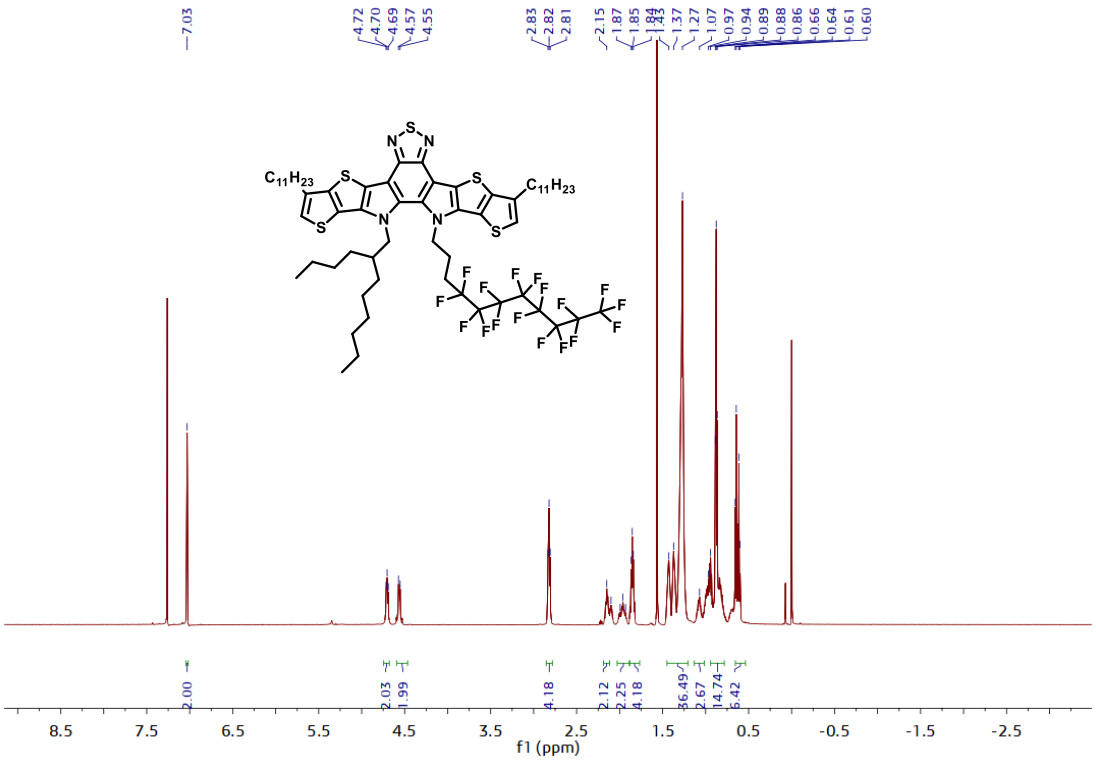

Figure S21. ^{1}H NMR spectrum of Compound 2b

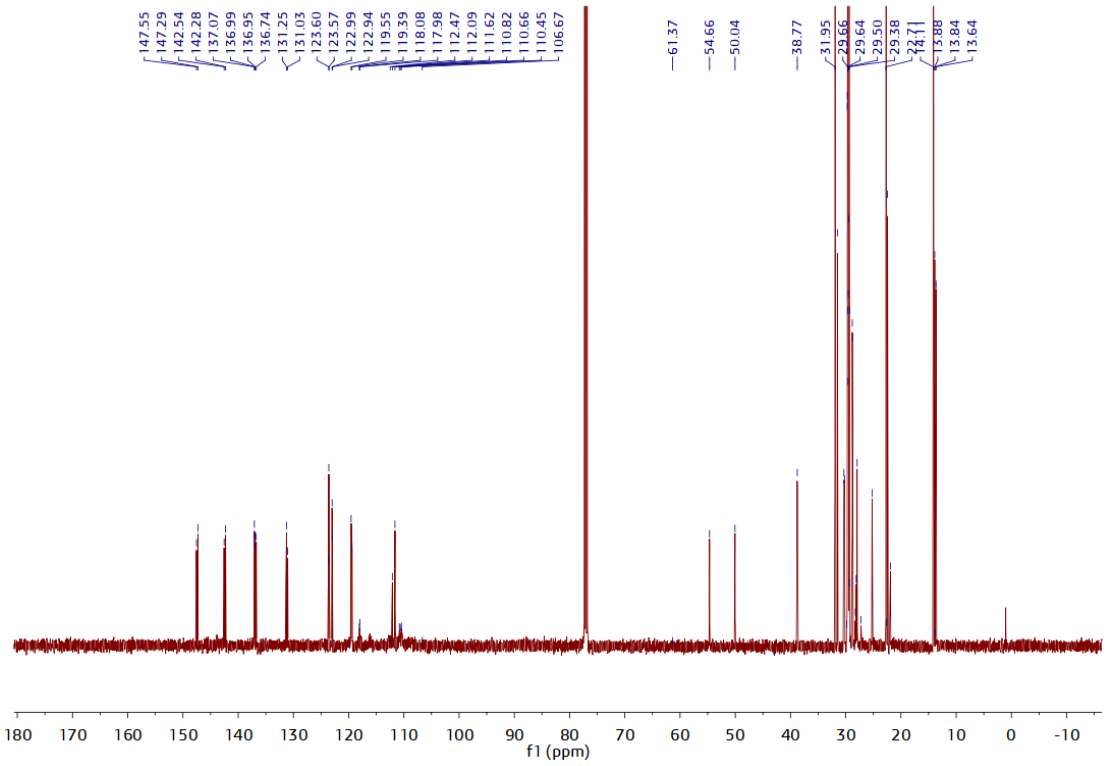

Figure S22. ^{13}C NMR spectrum of Compound 2b

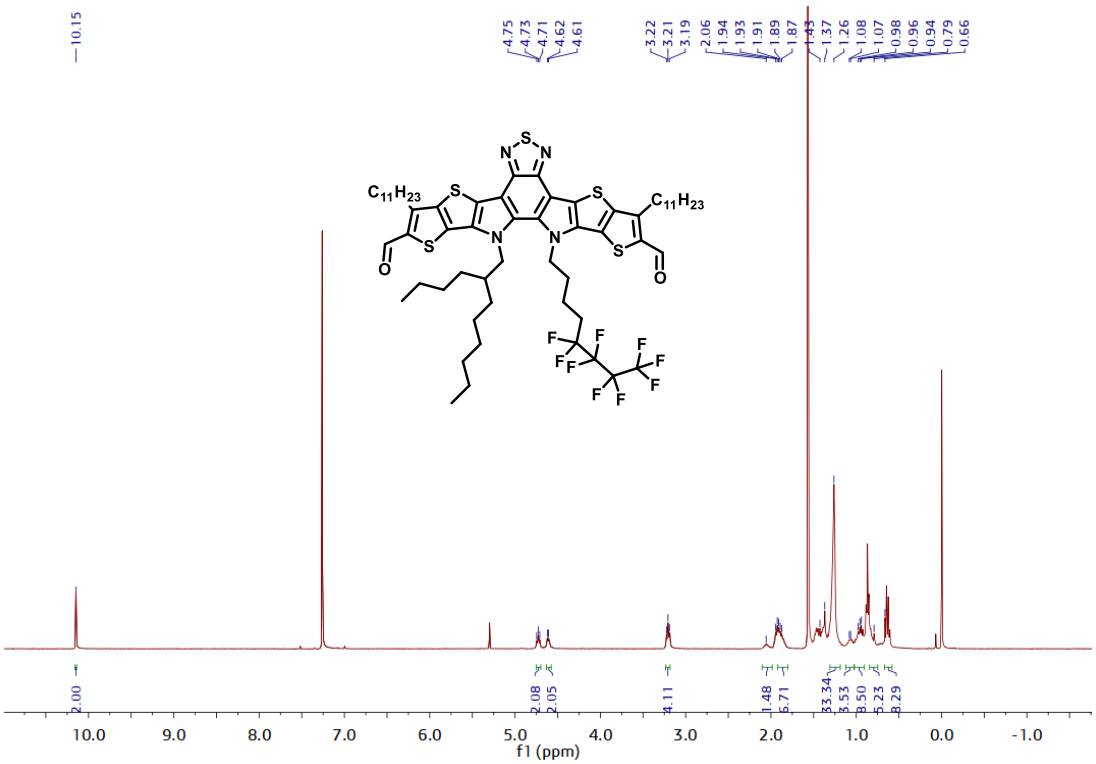

Figure S23. ^{1}H NMR spectrum of Compound 3a

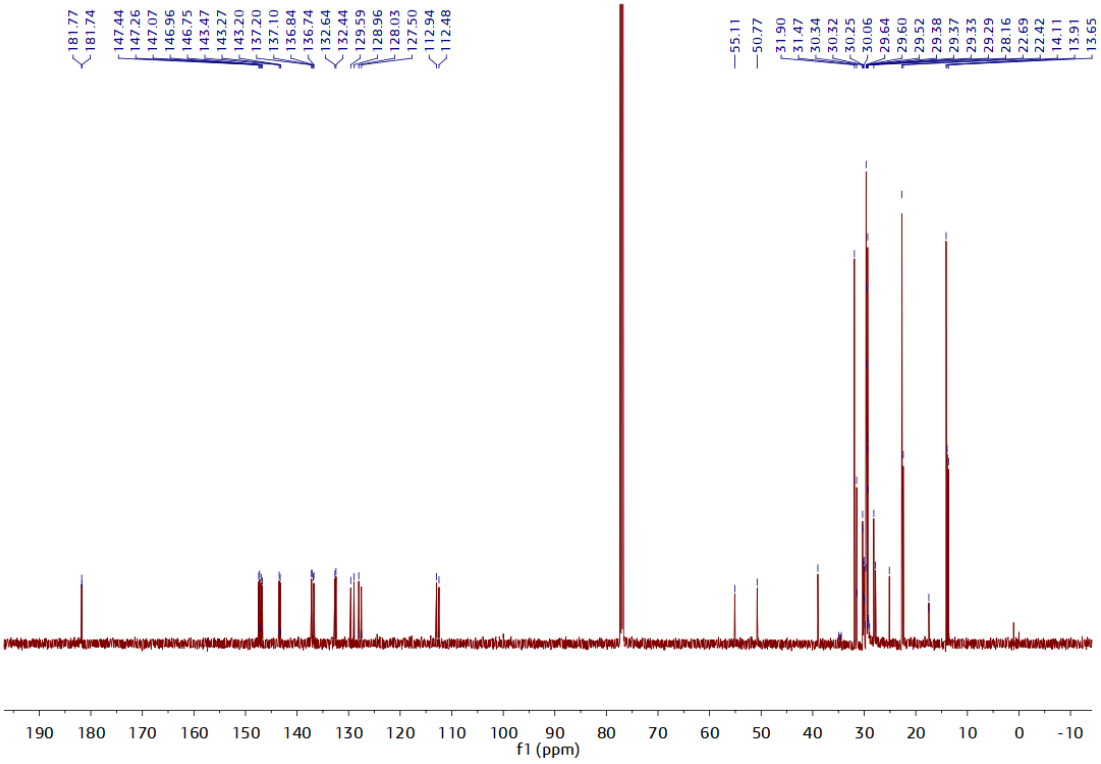

Figure S24. ^{13}C NMR spectrum of Compound 3a

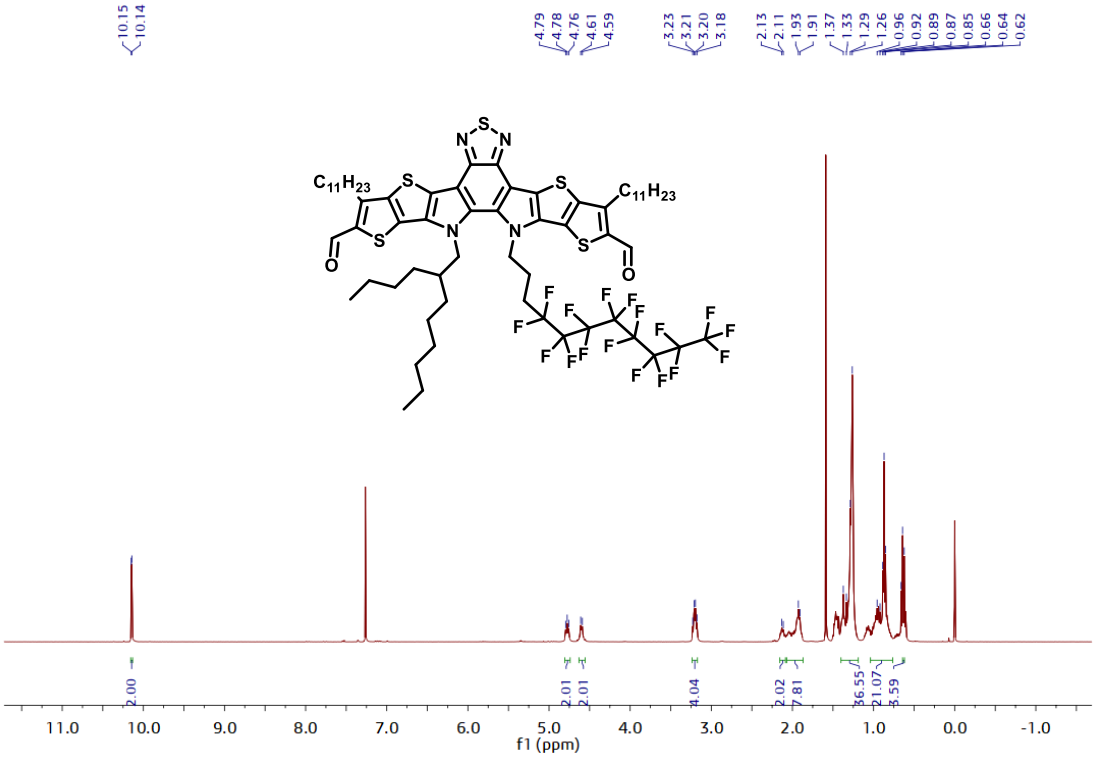

Figure S25. ^{1}H NMR spectrum of Compound 3b

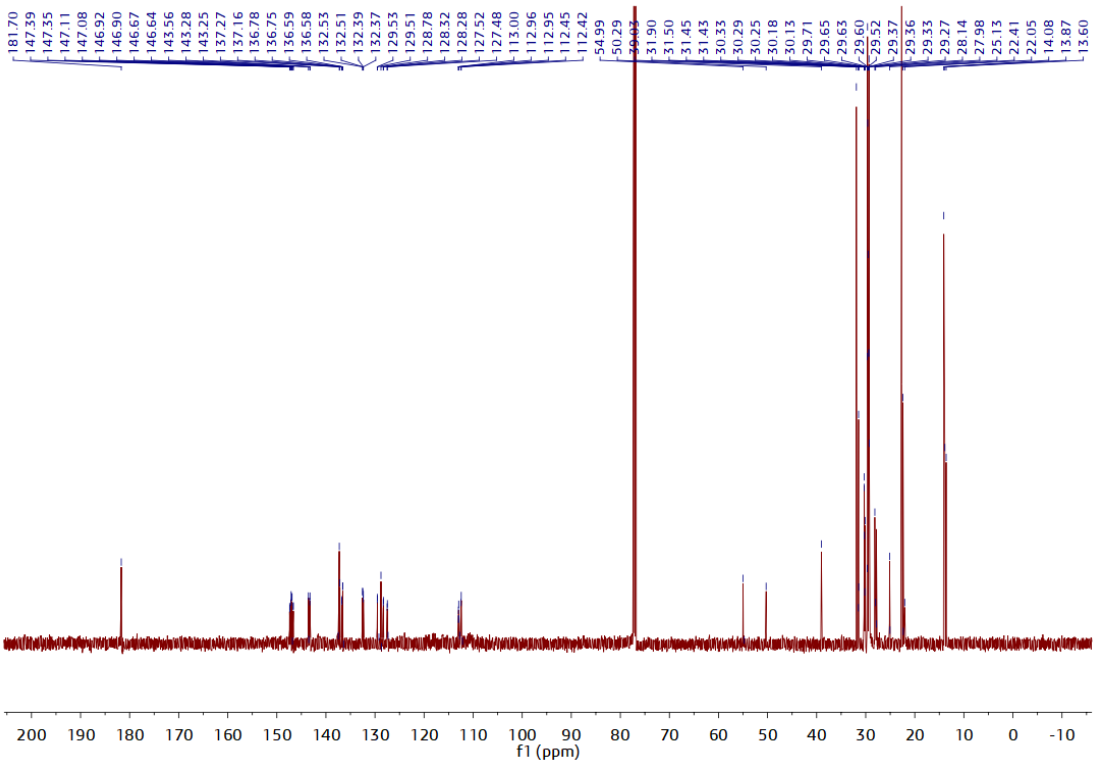

Figure S26. ^{13}C NMR spectrum of Compound 3b

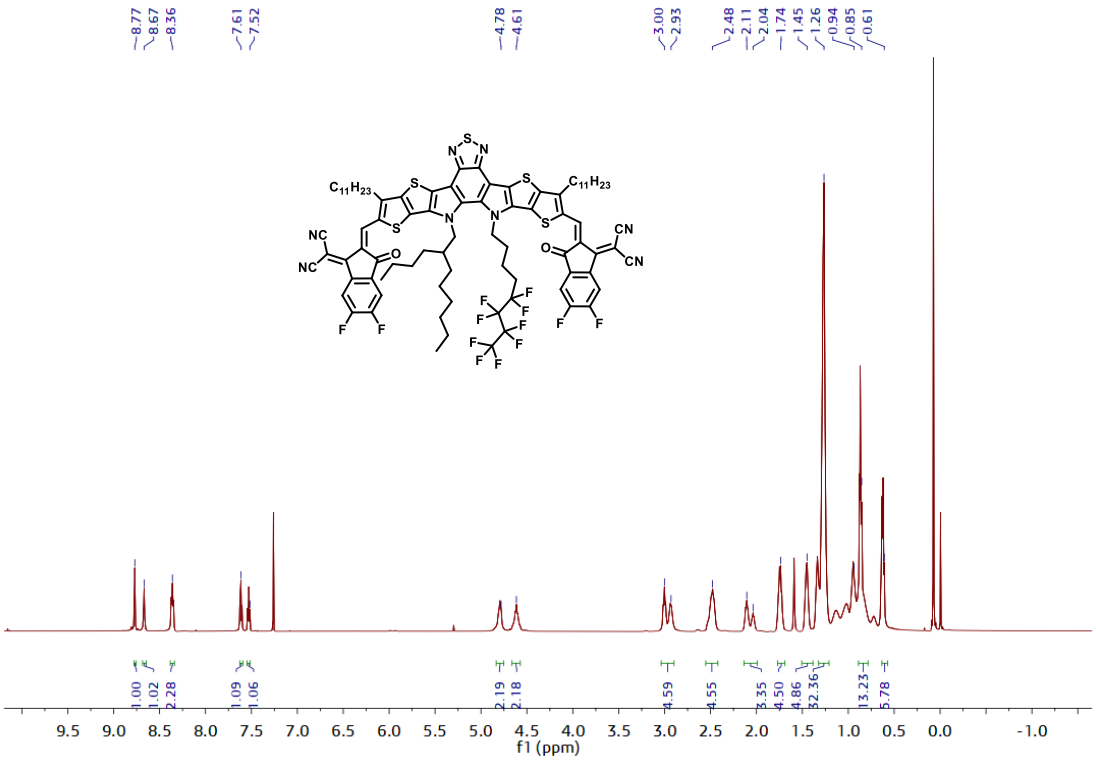

Figure S27. ^{1}H NMR spectrum of BTP-9F

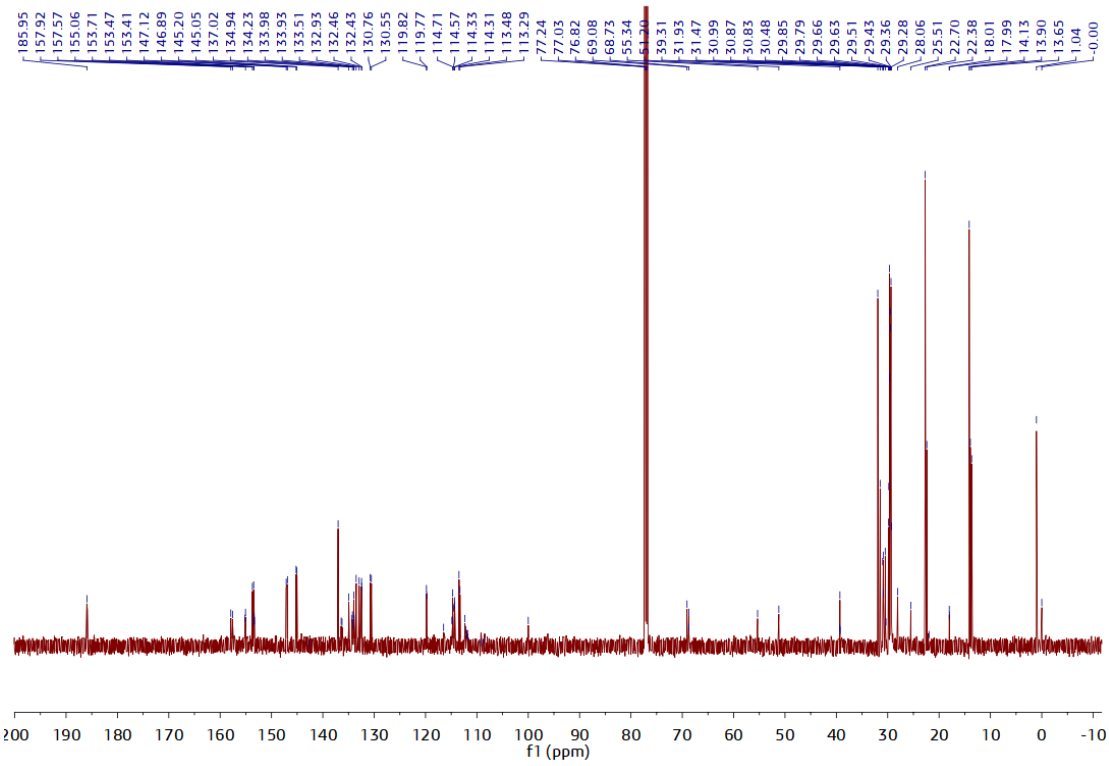

Figure S28 ^{13}C NMR spectrum of BTP-9F

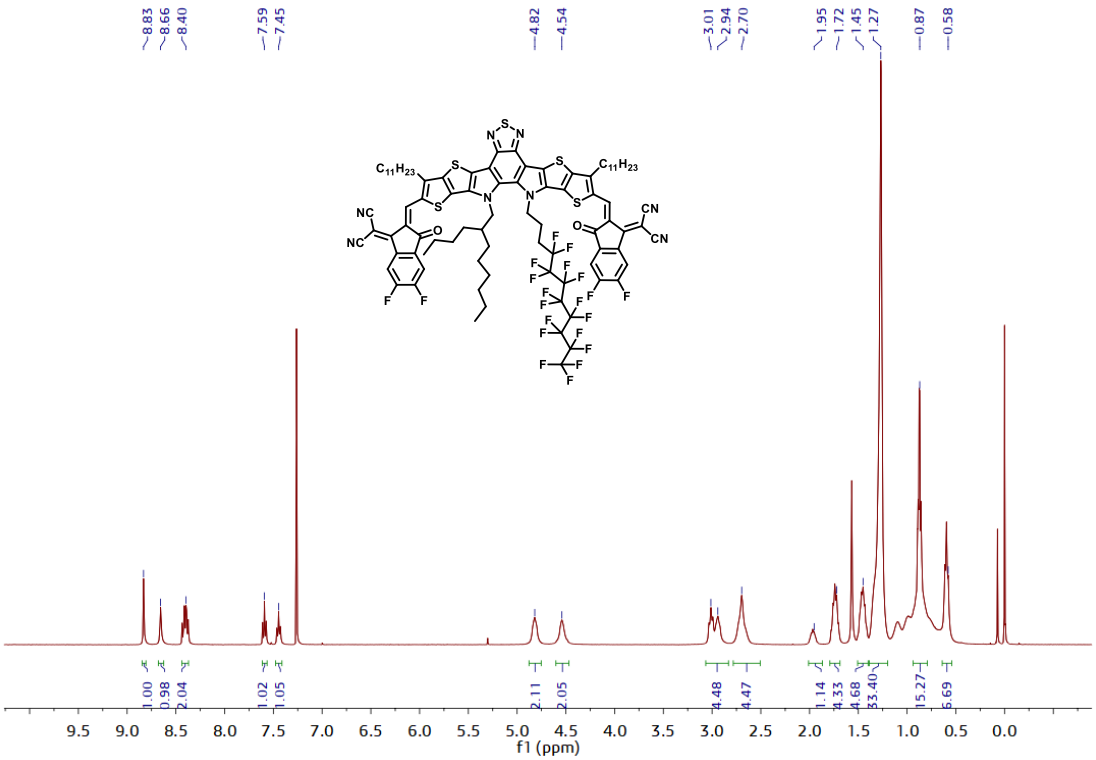

Figure S29. ^{1}H NMR spectrum of BTP-17F

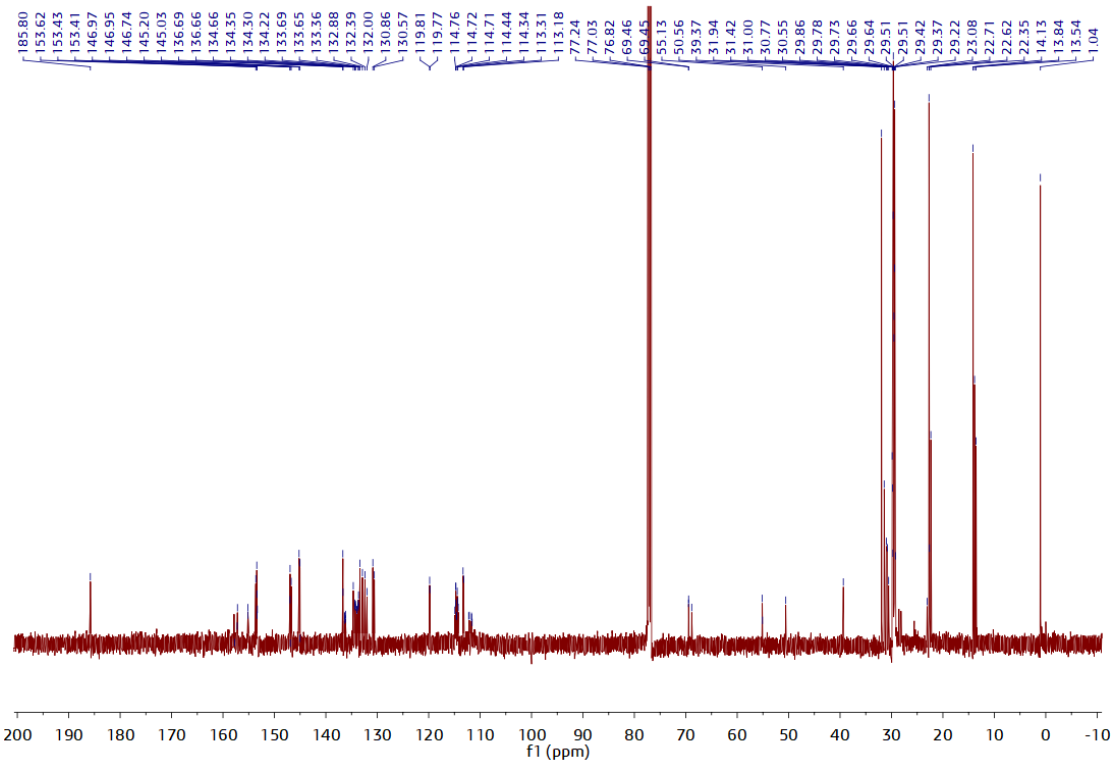

Figure S30. ^{13}C NMR spectrum of BTP-17F

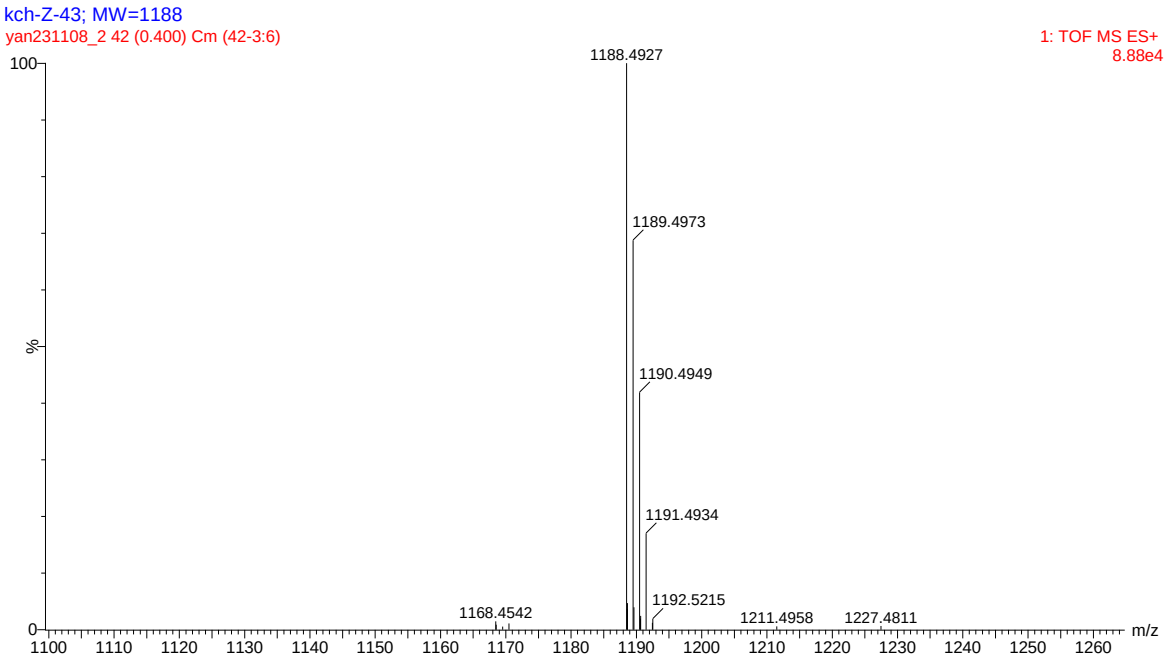

Figure S31. HR-MS spectrum of **2a**

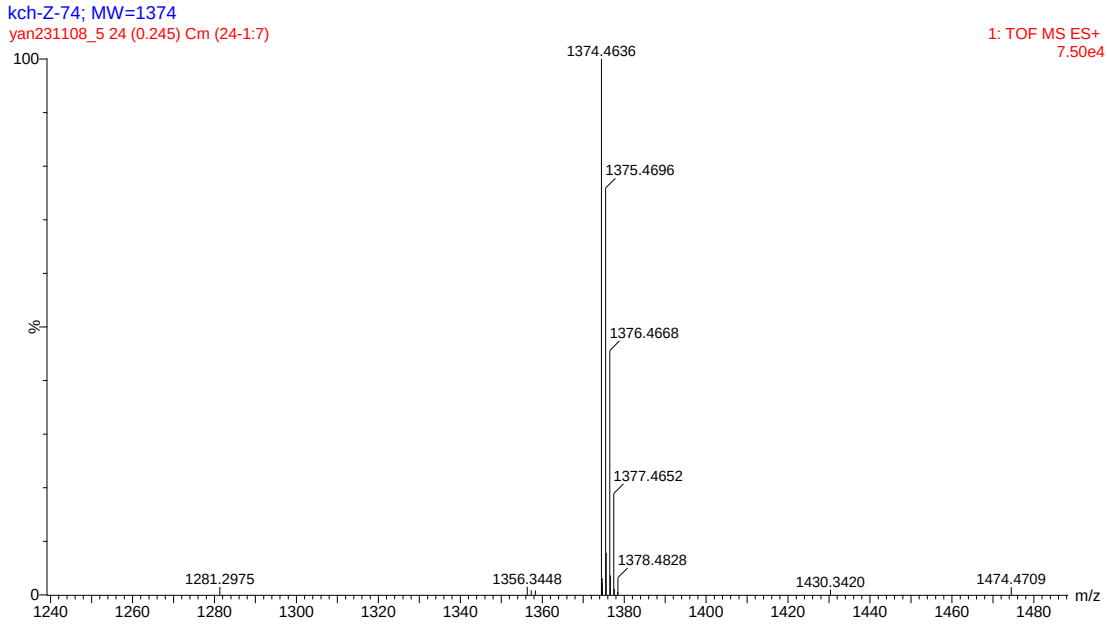

Figure S32. HR-MS spectrum of **2b**

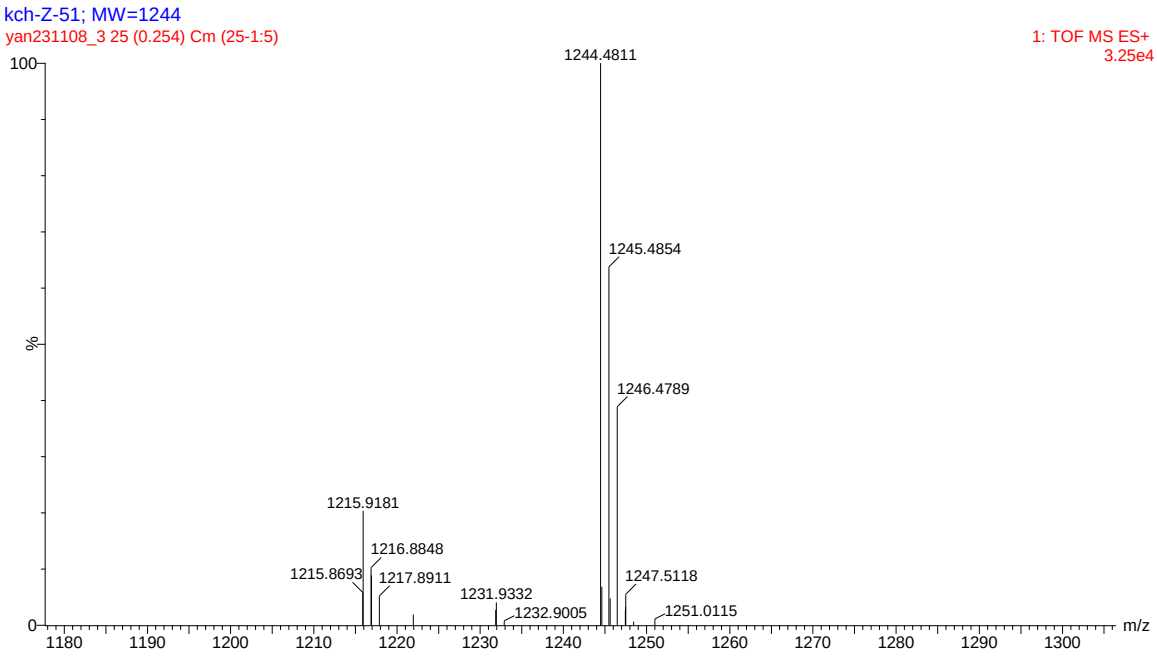

Figure S33. HR-MS spectrum of **3a**

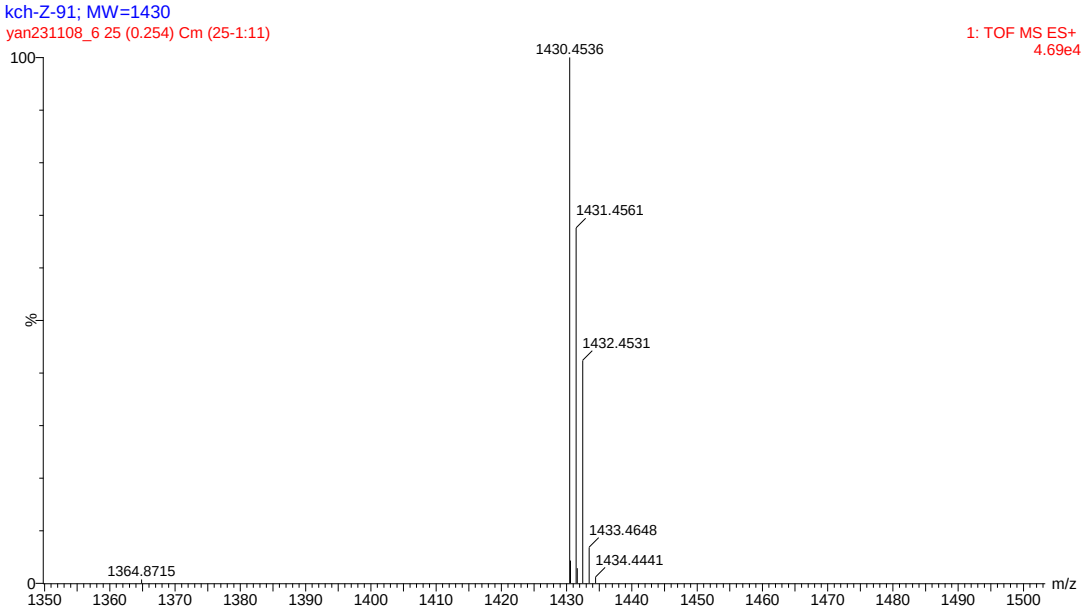

Figure S34. HR-MS spectrum of **3b**

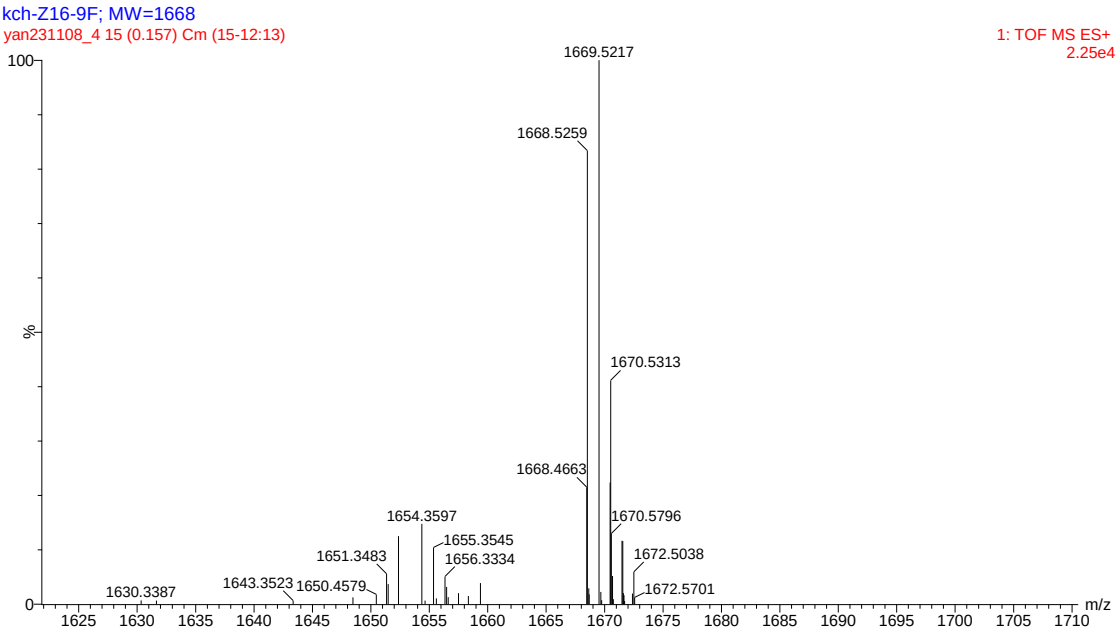

Figure S35. HR-MS spectrum of **BTP-9F**

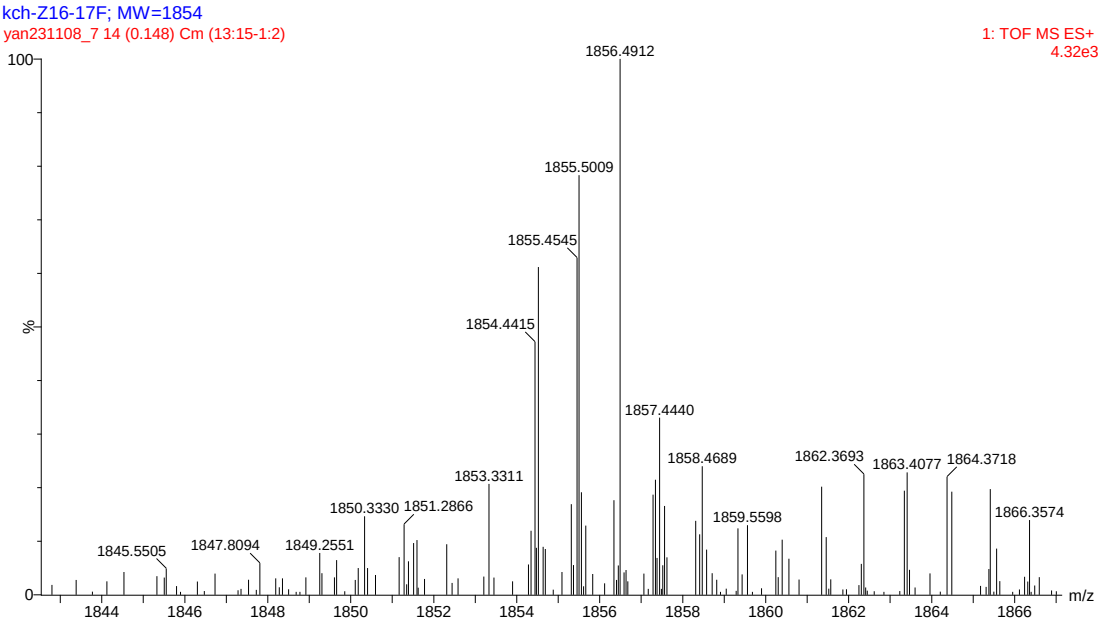

Figure S36. HR-MS spectrum of **BTP-17F**

References:

1. Zhang, Z.; Yang, L.; Hu, Z.; Yu, J.; Liu, X.; Wang, H.; Cao, J.; Zhang, F.; Tang, W., Charge density modulation on asymmetric fused-ring acceptors for high-efficiency photovoltaic solar cells. *Materials Chemistry Frontiers* **2020,** *4* (6), 1747-1755.

2. Dela Peña, T. A.; Khan, J. I.; Chaturvedi, N.; Ma, R.; Xing, Z.; Gorenflot, J.; Sharma, A.; Ng, F. L.; Baran, D.; Yan, H.; Laquai, F.; Wong, K. S., Understanding the Charge Transfer State and Energy Loss Trade-offs in Non-fullerene-Based Organic Solar Cells. *ACS Energy Lett.* **2021,** *6* (10), 3408-3416.

3. Hexemer, A.; Bras, W.; Glossinger, J.; Schaible, E.; Gann, E.; Kirian, R.; MacDowell, A.; Church, M.; Rude, B.; Padmore, H., A SAXS/WAXS/GISAXS Beamline with Multilayer Monochromator. *J. Phys. Conf. Ser.* **2010,** *247* (1), 012007.